
Article:
de Castro, Santiago Giménez, Lopes, João M. Viana Parente, Ferreira, Aires orcid.org/0000-0001-6017-8669 et al. (1 more author) (2024) Fast Fourier-Chebyshev Approach to Real-Space Simulations of the Kubo Formula. Physical Review Letters. 076302. ISSN: 1079-7114

https://doi.org/10.1103/PhysRevLett.132.076302

Fast Fourier-Chebyshev Approach to Real-Space Simulations of the Kubo Formula

Santiago Giménez de Castro,[1,2] João M. Viana Parente Lopes,[3] Aires Ferreira,[4,*] and D. A. Bahamon[1,2,†]

[1]School of Engineering, Mackenzie Presbyterian University, São Paulo - 01302-907, Brazil
[2]MackGraphe - Graphene and Nanomaterials Research Institute, Mackenzie Presbyterian University, São Paulo -01302-907, Brazil
[3]Centro de Física das Universidades do Minho e Porto, LaPMET, Departamento de Física e Astronomia, Faculdade de Ciências, Universidade do Porto, 4169-007 Porto, Portugal
[4]School of Physics, Engineering and Technology and York Centre for Quantum Technologies, University of York, York YO10 5DD, United Kingdom

(Received 16 July 2023; accepted 19 January 2024; published 16 February 2024)

The Kubo formula is a cornerstone in our understanding of near-equilibrium transport phenomena. While conceptually elegant, the application of Kubo's linear-response theory to interesting problems is hindered by the need for algorithms that are accurate and scalable to large lattice sizes beyond one spatial dimension. Here, we propose a general framework to numerically study large systems, which combines the spectral accuracy of Chebyshev expansions with the efficiency of divide-and-conquer methods. We use the hybrid algorithm to calculate the two-terminal conductance and the bulk conductivity tensor of 2D lattice models with over 10^7 sites. By efficiently sampling the microscopic information contained in billions of Chebyshev moments, the algorithm is able to accurately resolve the linear-response properties of complex systems in the presence of quenched disorder. Our results lay the groundwork for future studies of transport phenomena in previously inaccessible regimes.

DOI: 10.1103/PhysRevLett.132.076302

Chebyshev polynomials are a cornerstone of spectral approximation theory that have afforded unique numerical toolboxes for investigations of condensed matter [1]. Originally applied to overcome the limitations of power expansion methods in studies of atomic bonding in solids [2] and to accurately propagate wave packets in scattering problems [3], Chebyshev polynomial expansions of one- and two-particle correlation functions are nowadays routinely used to simulate equilibrium and dynamical properties of highly complex systems. This includes, among others, the simulation of localization in percolation models [4], rare-event effects in disordered semimetals [5,6], and excitations in strongly correlated matter [7–9].

A fundamental trait of spectral approximations is their built-in separation of thermodynamic variables, such as chemical potential and temperature, from the microscopic information encoded in the wave functions. A prototypical example is the density of states (DOS) at the Fermi energy [10,11]. Its Chebyshev expansion can be cast as $\nu(\varepsilon) = \Phi(\varepsilon)\sum_{n\geq 0}\mu_n T_n(\varepsilon)$, where $T_n(\varepsilon)$ and $\Phi(\varepsilon) = [\pi\sqrt{1-\varepsilon^2}]^{-1}$ are thermodynamic contributions standing for the nth Chebyshev polynomial and weight function in the dimensionless energy domain, respectively. Such an expansion, which is valid for any quantum system with a bounded spectrum, proves most efficient as the bulk of the computational effort is focused on the evaluation of the Chebyshev moments $\mu_n = \mathrm{Tr}[T_n(\hat{h})]$ (here, $\hat{h}$ is a suitably rescaled Hamiltonian with $\|\hat{h}\| \leq 1$). These moments (hosting the microscopic information) are obtained via a stable sequence of matrix-vector products—circumventing the need for costly exact diagonalization procedures—and stochastic trace estimators may be used to speed up the computation [12].

The computational complexity of spectral expansions of one-particle properties calculated for the general class of lattice models with short-range interactions is bounded favorably by $O(DM)$, where D is the Hilbert space dimension and M is the truncation order of the Chebyshev expansion. For noninteracting systems described by the tight-binding approximation, D is the total number of orbitals and thus the computational effort scales only linearly with the system size. This advantageous $O(DM)$ scaling has been leveraged to enable unprecedented fully non-perturbative studies of one-particle properties in disordered systems [13–21], but open questions remain regarding the possibility to handle two-particle properties (crucial for nonequilibrium studies) in an equally satisfactory fashion. Perhaps the most familiar among these is the electrical conductivity tensor, describing the charge current response to an external electric field [22]. The longitudinal dc response, $\sigma_{aa} \coloneqq \lim_{\omega\to 0}\sigma_{aa}(\omega)$ (with $a = x, y, z$), is only dependent on the electronic states at the Fermi energy (in the $T \to 0$ limit). Therefore, it turns out that σ_{aa} at the Fermi energy can be computed via the

Kubo-Greenwood formula with the same level of efficiency of a DOS calculation, courtesy of an *exact* Green's function Chebyshev polynomial expansion [13]. In other words, the number of arithmetic operations is favorably bounded by $O(DM)$. However, this strategy hinges upon the separability of the Chebyshev expansions of the retarded and advanced Green's functions in the dc Kubo-Greenwood conductivity due to containing only pure Fermi-surface terms. This is not warranted in more general scenarios, in which the Fermi sea of the electronic system plays a significant role (i.e., whenever the spectral representation of the response function contains off-Fermi surface contributions arising from transitions between filled and empty states). In fact, while the dc conductivity of time-reversal ($\mathcal{T}$) invariant systems is a *pure* Fermi-surface property, the breaking of the $\mathcal{T}$ symmetry changes this picture entirely [23]. A well-known example is the quantized anomalous Hall response of Chern insulators [24], which is determined by the Berry curvature of all occupied bands. Application of the spectral framework yields, in the general case, $\sigma_{ab} = \sum_{n,m} \Lambda^{nm} \mu_{ab;nm}$. Here, Λ^{nm} is a known function of the Fermi energy [13], $\mu_{ab;nm}$ is the trace of the special operator string $T_n(\hat{h})\hat{v}_a T_m(\hat{h})\hat{v}_b$ [1], and $\hat{\mathbf{v}}$ is the velocity operator. Evaluation of all the μ_{ab}^{nm} gives full-spectral access to the conductivity tensor, with any desired energy resolution provided M is large enough [13]. Unfortunately, such a task traditionally requires $O(DM^2)$ operations [25], which severely hampers the classes of problems that can be tackled.

In this Letter, we report linear-response transport simulations in graphene and bilayer graphene nanostructures that carry the spectral information of billions of double-Chebyshev expansion moments [i.e., $M^2 = O(10^{10})$]. This large-scale computational experiment is carried out with a new approach we present below, whose complexity scales with $DM \log M$ [in contrast to $O(DM^2)$] and hence entails a computational effort similar to a standard DOS calculation. This key improvement over the state of the art is shown to enable full-spectral calculations of the conductivity tensor with energy resolutions approaching the mean-level spacing of real systems.

Setting the stage.—We begin by briefly reviewing the main ingredients in the Chebyshev approach to real-space linear-response transport calculations. The dc conductivity at finite temperature may be cast as

$$\sigma_{ab}(\mu, T) = \frac{2e^2\hbar}{\pi\Omega} \Re \int dE\, f(E, \mu, T) \mathrm{Tr}[\hat{\mathcal{O}}_{ab}(E)], \quad (1)$$

where $f(E, \mu, T) = 1/[1 + e^{(E-\mu)/k_B T}]$, μ is the chemical potential, $\hat{\mathcal{O}}_{ab}(E) = i\hat{v}_a[\partial_E \hat{\mathcal{G}}(E)]\hat{v}_b \Im\hat{\mathcal{G}}(E)$ is the conductivity kernel operator, $\hat{\mathcal{G}}(E) = (E - \hat{H} + i0^+)^{-1}$ is the retarded Green's function, $\hat{H}$ is the real-space lattice Hamiltonian, $\hat{v}_a$ is the ath component of the velocity operator, and Ω is the d-dimensional volume [26]. $\hat{\mathcal{G}}(E)$ is approximated by a truncated Chebyshev expansion [13], smoothed by convolution with a kernel [1]. Hereafter, we focus the discussion on the diagonal dc conductivity and relegate the more general derivation to Ref. [27]. For efficiency, the trace in Eq. (1) is converted into a stochastic average over random vectors $\{|r\rangle\}_{r=1,\ldots,R}$ [12], according to

$$\sigma_{aa}(\mu, T) \simeq \frac{4e^2}{h\Omega} \int_{-1}^{1} d\varepsilon [-\partial_\varepsilon f(\varepsilon, \tilde{\mu}, \tilde{T})] \langle\langle \tilde{\sigma}_a^r(\varepsilon) \rangle\rangle_R, \quad (2)$$

where $\langle\langle \cdot \rangle\rangle_R$ denotes the statistical average with respect to the R random vectors and $\tilde{\sigma}_a^r(\varepsilon)$ is the contribution of a single random vector, formally given by

$$\tilde{\sigma}_a^r(\varepsilon) = \sum_{m,n=0}^{M-1} g_{mn}(\varepsilon) \mu_{a;mn}^r, \quad (3)$$

where $\mu_{a;mn}^r = \langle r|T_m(\hat{h})\tilde{v}_a T_n(\hat{h})\tilde{v}_a|r\rangle$, $\tilde{v}_a = \hbar\hat{v}_a/\Delta E$, $g_{nm}(\varepsilon) = g_m T_m(\varepsilon) g_n T_n(\varepsilon)/(1 - \varepsilon^2)$, and $\hat{h}$ and ε are rescaled versions of $\hat{H}$ and E, which map the eigenvalues of $\hat{H}$ and the energy onto the interval $[-1:1]$ (similar definitions apply to the rescaled temperature and chemical potential variables, $\tilde{\mu}$ and $\tilde{T}$). The error in the stochastic trace evaluation is negligible provided that $RD \gg 1$ [1], which is easily satisfied for the large systems considered here. As a rule of thumb, the relative root-mean-square fluctuation scales as $1/\sqrt{RD}$, and thus can be as low as 1% for just a single random vector realization of a system with $D = 10^4$ sites. Furthermore, ΔE is the energy bandwidth of the Hamiltonian and $g_m = 2K_m/[\pi(1 + \delta_{m,0})]$ encodes the kernel coefficients. In this work, the Jackson kernel [28] is adopted (see Ref. [29] for the explicit form of K_m). The spectral resolution is determined by the Gaussian width and satisfies $\delta E \leq \pi\Delta E/M$ [1].

The fast Fourier-Chebyshev algorithm (FastCheb).—From the definition of $\mu_{a;mn}^r$ we easily see that the total number of floating-point operations is $O(DM^2)$ for sparse Hamiltonians, validating our earlier claim. In what follows, we explore the powerful fast Fourier transform (FFT) algorithm [30,31] to improve the scalability.

First, we split the dimensionless energy interval $-1 \leq \varepsilon_k \leq 1$ into M energy points ε_k, with $k = 0, \ldots, M-1$. At each of these points, Eq. (3) for the kernel $\tilde{\sigma}_a^r(\varepsilon_k)$ can be rearranged as a scalar product between two energy dependent vectors [13]

$$\tilde{\sigma}_a^r(\varepsilon_k) = \frac{1}{1-\varepsilon_k^2}\left[\sum_{m=0}^{M-1} g_m T_m(\varepsilon_k)\langle a_m^{L;r}|\right] \cdot \left[\sum_{n=0}^{M-1} g_n T_n(\varepsilon_k)|a_n^{R;r}\rangle\right] = \frac{1}{1-\varepsilon_k^2}\langle \phi_{a;k}^{L;r}|\phi_{a;k}^{R;r}\rangle, \tag{4}$$

which we call left and right vectors. Moreover, we have introduced the auxiliary vectors $|a_m^{L;r}\rangle = T_m(\hat{h})|r\rangle$ and $|a_n^{R;r}\rangle = \tilde{v}_a T_n(\hat{h})\tilde{v}_a|r\rangle$ for compactness of notation. Next, the energy points are carefully chosen in order to match the nodes of the Chebyshev polynomials of the first kind, i.e.,$\varepsilon_k = \cos(\pi(k+1/2)/M)$. Exploiting the Chebyshev-to-Fourier mapping, $T_n(x) = \cos(n \arccos x)$, the right and left vectors at the ε_k points become

$$|\phi_{a;k}^{R/L;r}\rangle = \sum_{m=0}^{M-1} \frac{\cos(m\pi(k+1/2)/M)}{1+\delta_{m,0}} \frac{2K_m}{\pi} |a_m^{R/L;r}\rangle. \tag{5}$$

These are discrete cosine Fourier transforms of the vector sequences $K_m/\pi|a_m^{R/L;r}\rangle$, which is the main result of this Letter. We call these energy-space vectors.

Next, we employ a divide-and-conquer strategy to obtain all of the energy-space vectors *simultaneously* in an efficient manner. The key steps are as follows. First, we carry out the vector recursions and construct the matrices $\boldsymbol{a}_{L(R)}$ by lining up all vectors of the left (right) sequences $|a_n^{L(R)}\rangle$ along their columns. Then, we run through the matrices $\boldsymbol{a}_{L(R)}$, row by row, performing one-dimensional cosine FFTs. These FFTs yield the ith rows of the energy-space matrices as $\phi_{a;i,k}^{R/L;r} = \mathbf{FFT}^{m\to k}[K_m a_{i,m}^{R/L;r}/\pi]$ $(i = 1, \ldots, D)$. The partial result $p_{a;i}(\varepsilon_k)$ of the dot product from Eq. (4) is updated every time an energy-space row is obtained, i.e., $p_{a;i}(\varepsilon_k) = p_{a;i-1}(\varepsilon_k) + \phi_{a;i,k}^{L\dagger}\phi_{a;i,k}^{R}$. Finally, once all D rows have been visited, the random vector contribution is obtained as $\tilde{\sigma}_a^r(\varepsilon_k) = p_{a;D}(\varepsilon_k)/[\pi^2(1-\varepsilon_k^2)]$. The explicit evaluation of the M^2 Chebyshev moments $\{\mu_{a;mn}^r\}$ is bypassed. In its place, D FFTs of length M are performed, yielding a total of $O(DM\log M)$ operations.

Realizing the full extent of these advantages, however, requires that the $\boldsymbol{a}_{L(R)}$ are all stored in memory. That entails a memory cost $O(2DM)$, which is demanding for large systems [13]. To overcome this challenge, we employ a partitioning scheme which we discuss in detail in the Supplemental Material [27].

Implementation and benchmark.—In order to assess its baseline performance, *FastCheb* is implemented within framework of the open-source `KITE` code [16]. `KITE` is a high-performance code for spectral simulations of Green's functions and related quantities in real space [18,19], and

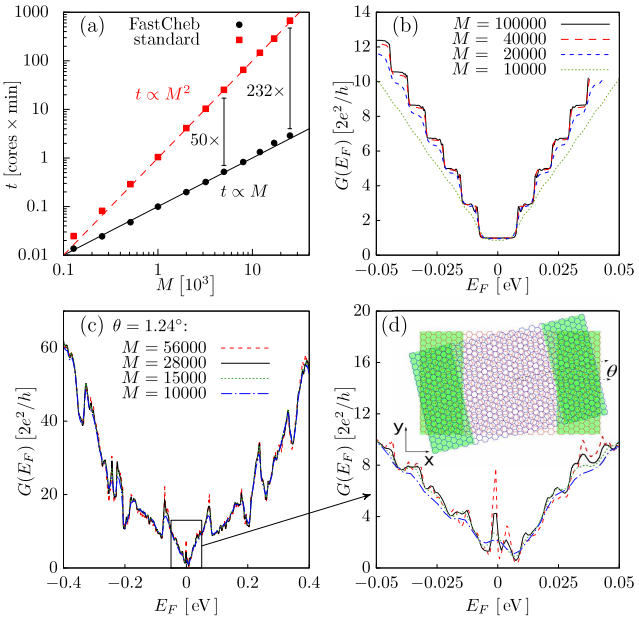

FIG. 1. (a) Scaling of CPU time with Chebyshev order M in the *FastCheb* and standard approaches. This benchmark is for a single random vector evaluation of σ_{xx} in a small system with 256×128 orbitals. (b) Fermi-energy dependence of the linear conductance of a large graphene nanoribbon with side lengths $L_x = L_y = 100$ nm, to which absorbing contacts of the same dimension are attached. The full TB model contains 10^7 orbitals. (c) and (d) Panoramic and detailed views of linear conductance curves for a TBG device with a total of 2.5×10^6 orbitals. Values of M corresponding to each curve in (b)–(d) are indicated on the plots. See Ref. [27] for more details.

hence is an ideal testbed for this study. The efficiency of our algorithm can be best appreciated in a direct comparison with the standard recursive method. To this end, we simulate the diagonal conductivity of graphene using a minimal nearest-neighbor tight-binding (TB) model on a honeycomb lattice. The results of this benchmark are summarized in Fig. 1(a), where the computational effort is seen to follow closely the behavior expected from the earlier considerations. In this example, the calculation with 5000 Chebyshev moments using *FastCheb* is 50 times faster compared to the standard approach, while for $M = 25\,000$ it has already become 232 times faster. This M-scaling law for the CPU time is robust and representative of a wide class of problems. By the way of two main case studies, we show below that *FastCheb* has pivotal advantages in linear-response studies of bulk electrical conductivity and conductance in nanostructures.

Ballistic conductance and twisting effects.—We start by simulating a two-terminal quantum-transport device made from a large graphene nanoribbon. The linear conductance at the Fermi energy, $G(E_F)$, is obtained from the $T \to 0$ limit of Eq. (2) [$\sigma_{aa}(E_F) \simeq (4e^2/h\Omega)\langle\langle\tilde{\sigma}_a^r(\varepsilon_F)\rangle\rangle_R$] using the framework for two-terminal devices recently developed in

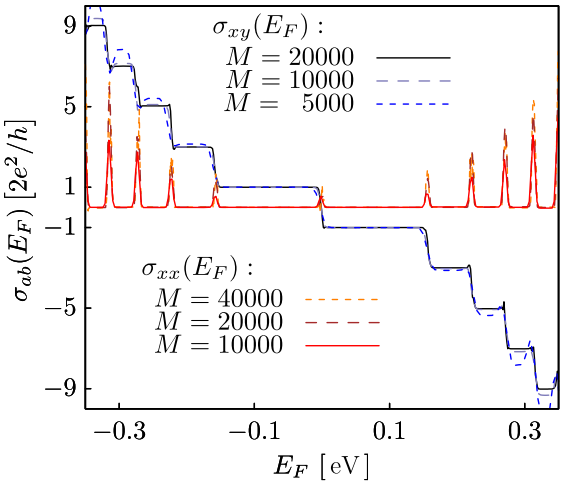

FIG. 2. Longitudinal and transverse conductivity as function of the Fermi energy in a disordered graphene system tuned to the quantum Hall regime. The lattice has a total of 10^7 sites. The parameters are set to $W = 0.1t$ (disorder strength), with $t = 2.7$ eV (nearest-neighbor hopping energy), and magnetic flux $\Phi \simeq 3 \times 10^{-4} h/e$. Data are averaged over 10 random-vector and 4 disorder realizations. Periodic boundary conditions are employed.

Ref. [32]. Note that in the zero-temperature limit, this quantity is a pure Fermi surface property and the conductivity kernel directly yields the dc response. The linear conductance is known to exhibit well-defined quantization steps due the transverse subbands formed in confined nanostructures. The changes in the conductance occur in discrete steps of e^2/h (per spin) each time a new transport channel opens up at the Fermi level [33,34]. Figure 1(b) shows that this behavior is fully captured by the spectral algorithm, with the Chebyshev truncation order playing a central role. Because the plateau width is so small (around 1 meV), tens of thousands of iterations are required to accurately reproduce sharp step changes in the conductance. This can be traced back to the slow algebraic convergence generated by steplike discontinuities, one of the hardest singularities to resolve with polynomial expansions [35]. Thanks to the efficiency of *FastCheb*, such fine features can be captured with modest computational effort.

Next, we demonstrate the power of our algorithm by resolving the linear-response conductance of large twisted bilayer graphene (TBG) devices. We focus on commensurate structures with small twist angle θ, modelled via a Slater-Koster tight-binding scheme [36,37]. To faithfully capture interlayer interactions in TBG, it is imperative to go beyond a nearest-neighbor approximation [38]. Here, we include full hopping integrals up to a distance of 0.58 nm (approximately four times the bond length). In practice this entails around 60 neighbors for each carbon atom, which makes a transport study prohibitively demanding for exact diagonalization. The conductance of a TBG device with $\theta = 1.24°$ obtained with *FastCheb* is shown in Figs. 1(c) and 1(d). Owing to the full-spectral capability of the algorithm, it is possible to zoom in on small features, such as the conductance peak at the charge neutrality point caused by residual dispersion of the conduction bands. The absence of ballistic conductance steps is due to the channel mixing caused by elastic scattering between the layers, and is thus a direct result of moiré supercell effects [32]. Based on our extensive tests, we estimate that the largest TBG simulation (i.e., $M = 56\,000$, corresponding to a spectral resolution of 0.5 meV, and taking 40 core hours with *FastCheb*), would require around 2400 core hours using the standard kernel polynomial approach.

Kubo-Bastin formulation: Hall conductivity.—The key motivation for developing *FastCheb* is to extend the range of transport phenomena that can be studied by means of microscopic lattice models. It is well known that many facets of disordered systems and quantum criticality are notoriously challenging to address numerically even at the level of one-particle properties (such as the inverse localization length [39,40]). An example is the scaling behavior of integer quantum Hall transitions that remains a long-standing problem, with most recent progress making use of transfer-matrix calculations in quasi-1D geometry [41–44]. The possibility to perform large-scale lattice calculations of the full conductivity tensor in 2D geometry makes *FastCheb* a promising tool in quantum transport. Here, a start is made towards the application of such a tool to quantum Hall systems. The Kubo-Bastin formalism is employed for this purpose because it provides a unified treatment of all components of the conductivity tensor [26] and is amenable to spectral expansions [16,25,27,45].

We choose the integer quantum Hall effect in graphene to demonstrate the capacity of *FastCheb* to probe topological transport in large 2D systems. The Hall conductivity in graphene obeys an unconventional quantization condition, $\sigma_{xy}^n = \mp\, 2e^2/h(2n+1)$ with $n \in \mathbb{Z}_0^+$ (here, the $\pm$ signs hold for electrons or holes), due the Berry phase of the electron wave functions [46–48]. The numerical implementation of the Kubo-Bastin formula revolves around the same concepts as before, however this time 6 energy-space vectors are required (as opposed to two for pure Fermi surface quantities like the $T = 0$ longitudinal conductivity). The perpendicular magnetic field is included in the Hamiltonian through Peierls's phases in the hopping terms, generating a magnetic flux Φ per unit cell. To emulate the effect of disorder, we supplement the TB Hamiltonian with an uncorrelated on-site potential [16].

The longitudinal (xx) and Hall (xy) conductivity of a large system with side lengths $L_x = 1600$ and $L_y = 3200$ (in units of the lattice spacing) is shown in Fig. 2. Both quantities are seen to follow the expected behavior for the insulating quantum Hall regime of graphene [46], thus validating the robustness of the new approach. We emphasize again that the large values of M—required to resolve sharp features satisfactorily—are out of reach for previous

methods due to their inherent $O(DM^2)$ scaling [16,21,25]. *FastCheb* offers the possibility of evaluating $\sigma_{xy}(E)$ with high precision and energy resolution, as demonstrated here, being an order-$DM \log M$ approach. In fact, its full-spectral capability is essential to capture the intrinsic Hall conductivity due to being a bulk Fermi sea property. This contrasts with the case of the longitudinal conductivity (a bulk Fermi surface property) where studies for a small grid of Fermi energies can be carried out efficiently with the single-shot algorithm [13]. Here, the unique advantage of *FastCheb* lies in the ability to efficiently reconstruct $\sigma_{aa}(E)$ over the *full* spectrum. In our studies, speed-ups of up to 100 over the standard method are achieved [27].

Final remarks.—Applying the fast Fourier-Chebyshev algorithm to the study of quantum-critical phenomena can be a starting point for future research. Specifically, the investigation of the scaling behavior of Anderson transitions (such as metal-to-insulator and integer quantum Hall transitions [49]) could benefit enormously from the spectral machinery developed in this work. In fact, the size of the lattice in our 2D conductance study [see Figs. 1(b)–1(d)] is already larger than recent calculations for semiclassical network models [50], which is promising. *FastCheb* could also facilitate finite-size scaling analysis of the Hall conductivity, far less studied numerically than the diagonal response but equally important.

S. G. d. C. and D. A. B. acknowledge support from CAPES (88887.510399/2020-00), CAPES-PRINT (88887.310281/2018-00, 88887.899997/2023-00), CNPq (309835/2021-6), and Mackpesquisa. Supercomputer time was provided on MackCloud and Viking (University of York). J. M. V. P. L. acknowledges the Centro de Física do Porto funded by the Portuguese Foundation for Science and Technology (FCT) within the Strategic Funding UIDB/04650/2020. A. F. acknowledges support from the Royal Society (URF\R\191021 and RF\ERE\210281). S. G. d. C. is grateful to Jesuel Marques Leal Junior and Carlos Guillermo Giménez de Castro for useful discussions.

*aires.ferreira@york.ac.uk
†dario.bahamon@mackenzie.br

[1] A. Weiße, G. Wellein, A. Alvermann, and H. Fehske, The kernel polynomial method, Rev. Mod. Phys. **78**, 275 (2006).
[2] J. C. Wheeler and C. Blumstein, Modified moments for harmonic solids, Phys. Rev. B **6**, 4380 (1972).
[3] H. TalEzer and R. Kosloff, An accurate and efficient scheme for propagating the time dependent Schrödinger equation, J. Chem. Phys. **81**, 3967 (1984).
[4] G. Schubert, A. Weiße, and H. Fehske, Localization effects in quantum percolation, Phys. Rev. B **71**, 045126 (2005).
[5] J. H. Pixley, D. A. Huse, and S. Das Sarma, Rare-region-induced avoided quantum criticality in disordered three-dimensional Dirac and Weyl semimetals, Phys. Rev. X **6**, 021042 (2016).
[6] J. P. Santos Pires, B. Amorim, A. Ferreira, I. Adagideli, E. R. Mucciolo, and J. M. Viana Parente Lopes, Breakdown of universality in three-dimensional Dirac semimetals with random impurities, Phys. Rev. Res. **3**, 013183 (2021).
[7] A. Holzner, A. Weichselbaum, I. P. McCulloch, U. Schollwöck, and J. von Delft, Chebyshev matrix product state approach for spectral functions, Phys. Rev. B **83**, 195115 (2011).
[8] F. A. Wolf, J. A. Justiniano, I. P. McCulloch, and U. Schollwöck, Spectral functions and time evolution from the Chebyshev recursion, Phys. Rev. B **91**, 115144 (2015).
[9] D. Hendry, H. Chen, P. Weinberg, and A. E. Feiguin, Chebyshev expansion of spectral functions using restricted Boltzmann machines, Phys. Rev. B **104**, 205130 (2021).
[10] R. N. Silver and H. Röder, Calculation of densities of states and spectral functions by Chebyshev recursion and maximum entropy, Phys. Rev. E **56**, 4822 (1997).
[11] A. Ferreira, J. Viana-Gomes, J. Nilsson, E. R. Mucciolo, N. M. R. Peres, and A. H. Castro Neto, Unified description of the dc conductivity of monolayer and bilayer graphene at finite densities based on resonant scatterers, Phys. Rev. B **83**, 165402 (2011).
[12] T. Iitaka and T. Ebisuzaki, Algorithm for linear response functions at finite temperatures: Application to ESR spectrum of $s = \frac{1}{2}$ antiferromagnet Cu benzoate, Phys. Rev. Lett. **90**, 047203 (2003).
[13] A. Ferreira and E. R. Mucciolo, Critical delocalization of chiral zero energy modes in graphene, Phys. Rev. Lett. **115**, 106601 (2015).
[14] G. Bouzerar, S. Thébaud, S. Pecorario, and C. Adessi, Drastic effects of vacancies on phonon lifetime and thermal conductivity in graphene, J. Phys. Condens. Matter **32**, 295702 (2020).
[15] D. Varjas, M. Fruchart, A. R. Akhmerov, and P. M. Perez-Piskunow, Computation of topological phase diagram of disordered $Pb_{1-x}Sn_xTe$ using the kernel polynomial method, Phys. Rev. Res. **2**, 013229 (2020).
[16] M. J. Simão, M. Andelković, L. Covaci, T. G. Rappapport, J. P. Lopes, and A. Ferreira, KITE: High-performance accurate modelling of electronic structure and response functions of large molecules, disordered crystals and heterostructures, R. Soc. Open Sci. **7**, 191809 (2020).
[17] T. Löthman, C. Triola, J. Cayao, and A. M. Black-Schaffer, Efficient numerical method for evaluating normal and anomalous time-domain equilibrium Green's functions in inhomogeneous systems, Phys. Rev. B **104**, 125405 (2021).
[18] J. P. Santos Pires, S. M. João, A. Ferreira, B. Amorim, and J. M. Viana Parente Lopes, Anomalous transport signatures in Weyl semimetals with point defects, Phys. Rev. Lett. **129**, 196601 (2022).
[19] S. M. João, J. M. V. P. Lopes, and A. Ferreira, High-resolution real-space evaluation of the self-energy operator of disordered lattices: Gade singularity, spin-orbit effects and p-wave superconductivity, J. Phys. **5**, 045002 (2022).
[20] X. Liu, G. Farahi, C.-L. Chiu, Z. Papic, K. Watanabe, T. Taniguchi, M. P. Zaletel, and A. Yazdani, Visualizing broken symmetry and topological defects in a quantum Hall ferromagnet, Science **375**, 321 (2022).
[21] Z. Fan, J. H. Garcia, A. W. Cummings, J. E. Barrios-Vargas, M. Panhans, A. Harju, F. Ortmann, and S. Roche, Linear

scaling quantum transport methodologies, Phys. Rep. **903**, 1 (2021), linear scaling quantum transport methodologies.
[22] G. D. Mahan, *Many Particle Physics*, 3rd ed. (Plenum, New York, 2000).
[23] H. U. Baranger and A. D. Stone, Electrical linear-response theory in an arbitrary magnetic field: A new Fermi-surface formation, Phys. Rev. B **40**, 8169 (1989).
[24] F. D. M. Haldane, Berry curvature on the Fermi surface: Anomalous Hall effect as a topological Fermi-liquid property, Phys. Rev. Lett. **93**, 206602 (2004).
[25] J. H. García, L. Covaci, and T. G. Rappoport, Real-space calculation of the conductivity tensor for disordered topological matter, Phys. Rev. Lett. **114**, 116602 (2015).
[26] A. Bastin, C. Lewiner, O. Betbeder-matibet, and P. Nozieres, Quantum oscillations of the Hall effect of a fermion gas with random impurity scattering, J. Phys. Chem. Solids **32**, 1811 (1971).
[27] See Supplemental Material at http://link.aps.org/supplemental/10.1103/PhysRevLett.132.076302 for the derivation of energy-space vectors in the Kubo-Bastin formulation, and for additional details on the simulations and the partitioning scheme employed to mitigate the memory cost.
[28] D. Jackson, On approximation by trigonometric sums and polynomials, Trans Am. Math. Soc. **13**, 491 (1912).
[29] $k_m = [(M-m+1)/M+1]\cos[\pi m/(M+1)] + \sin[\pi m/(M+1)]\cot[\pi m/(M+1)]$.
[30] J. W. Cooley, P. Lewis, and P. Welch, The fast Fourier transform and its applications, IEEE Trans Educ. **12**, 28 (1969).
[31] M. Frigo and S. Johnson, The design and implementation of FFTW3, Proc. IEEE **93**, 216 (2005).
[32] S. G. de Castro, A. Ferreira, and D. A. Bahamon, Efficient Chebyshev polynomial approach to quantum conductance calculations: Application to twisted bilayer graphene, Phys. Rev. B **107**, 045418 (2023).
[33] B. J. van Wees, H. van Houten, C. W. J. Beenakker, J. G. Williamson, L. P. Kouwenhoven, D. van der Marel, and C. T. Foxon, Quantized conductance of point contacts in a two-dimensional electron gas, Phys. Rev. Lett. **60**, 848 (1988).
[34] D. A. Wharam, T. J. Thornton, R. Newbury, M. Pepper, H. Ahmed, J. E. F. Frost, D. G. Hasko, D. C. Peacock, D. A. Ritchie, and G. A. C. Jones, One-dimensional transport and the quantisation of the ballistic resistance, J. Phys. C **21**, L209 (1988).
[35] J. P. Boyd, *Chebyshev and Fourier Spectral Methods* (Dover Publications, Inc, New York, 2000).
[36] J. C. Slater and G. F. Koster, Simplified LCAO method for the periodic potential problem, Phys. Rev. **94**, 1498 (1954).
[37] D. A. Bahamon, G. Gómez-Santos, and T. Stauber, Emergent magnetic texture in driven twisted bilayer graphene, Nanoscale **12**, 15383 (2020).
[38] P. Moon and M. Koshino, Energy spectrum and quantum Hall effect in twisted bilayer graphene, Phys. Rev. B **85**, 195458 (2012).
[39] B. Kramer and A. MacKinnon, Localization: Theory and experiment, Rep. Prog. Phys. **56**, 1469 (1993).
[40] K. Slevin and T. Ohtsuki, Critical exponent for the quantum Hall transition, Phys. Rev. B **80**, 041304(R) (2009).
[41] H. Obuse, I. A. Gruzberg, and F. Evers, Finite-size effects and irrelevant corrections to scaling near the integer quantum Hall transition, Phys. Rev. Lett. **109**, 206804 (2012).
[42] I. A. Gruzberg, A. Klümper, W. Nuding, and A. Sedrakyan, Geometrically disordered network models, quenched quantum gravity, and critical behavior at quantum Hall plateau transitions, Phys. Rev. B **95**, 125414 (2017).
[43] M. Puschmann, P. Cain, M. Schreiber, and T. Vojta, Integer quantum Hall transition on a tight-binding lattice, Phys. Rev. B **99**, 121301(R) (2019).
[44] K. Slevin and T. Ohtsuki, Irrelevant corrections at the quantum Hall transition, Phys. Status Solidi (RRL)—Rapid Res. Lett. **17** 2300080 (2023).
[45] J. H. Garcia, J. You, M. García-Mota, P. Koval, P. Ordejón, R. Cuadrado, M. J. Verstraete, Z. Zanolli, and S. Roche, Electrical control of spin-polarized topological currents in monolayer WTe_2, Phys. Rev. B **106**, L161410 (2022).
[46] V. P. Gusynin and S. G. Sharapov, Unconventional integer quantum Hall effect in graphene, Phys. Rev. Lett. **95**, 146801 (2005).
[47] Y. Zhang, Y.-W. Tan, H. L. Stormer, and P. Kim, Experimental observation of the quantum Hall effect and Berry's phase in graphene, Nature (London) **438**, 201 (2005).
[48] K. S. Novoselov, A. K. Geim, S. V. Morozov, D. Jiang, M. I. Katsnelson, I. V. Grigorieva, S. V. Dubonos, and A. A. Firsov, Two-dimensional gas of massless Dirac fermions in graphene, Nature (London) **438**, 197 (2005).
[49] F. Evers and A. D. Mirlin, Anderson transitions, Rev. Mod. Phys. **80**, 1355 (2008).
[50] E. J. Dresselhaus, B. Sbierski, and I. A. Gruzberg, Scaling collapse of longitudinal conductance near the integer quantum Hall transition, Phys. Rev. Lett. **129**, 026801 (2022).